Structure and stability of the magnetic solar tachocline

To cite this article: G Rüdiger and L L Kitchatinov 2007 *New J. Phys.* **9** 302

New Journal of Physics
The open–access journal for physics

Structure and stability of the magnetic solar tachocline

G Rüdiger[1,3] **and L L Kitchatinov**[1,2]

[1] Astrophysikalisches Institut Potsdam, An der Sternwarte 16, D-14482, Potsdam, Germany
[2] Institute for Solar-Terrestrial Physics, PO Box 4026, Irkutsk 664033, Russia
E-mail: gruediger@aip.de and kit@iszf.irk.ru

New Journal of Physics **9** (2007) 302
Received 4 January 2007
Published 31 August 2007
Online at http://www.njp.org/
doi:10.1088/1367-2630/9/8/302

Abstract. Rather weak fossil magnetic fields in the radiative core can produce the solar tachocline if the field is almost horizontal in the tachocline region, i.e. if the field is confined within the core. This particular field geometry is shown to result from a shallow ($\lesssim$1 Mm) penetration of the meridional flow existing in the convection zone into the radiative core. Two conditions are thus crucial for a magnetic tachocline theory: (i) the presence of meridional flow of a few metres per second at the base of the convection zone, and (ii) a magnetic diffusivity inside the tachocline smaller than 10^8 cm^2 s^{-1}. Numerical solutions for the confined poloidal fields and the resulting tachocline structures are presented. We find that the tachocline thickness runs as $B_{\rm p}^{-1/2}$ with the poloidal field amplitude falling below 5% of the solar radius for $B_{\rm p} > 5$ mG. The resulting toroidal field amplitude inside the tachocline of about 100 G does not depend on the $B_{\rm p}$. The hydromagnetic stability of the tachocline is only briefly discussed. For the hydrodynamic stability of latitudinal differential rotation we found that the critical 29% of the 2D theory of Watson (1981 *Geophys. Astrophys. Fluid Dyn.* **16** 285) are reduced to only 21% in 3D for marginal modes of about 6 Mm radial scale.

[3] Author to whom any correspondence should be addressed.

PII: S1367-2630(07)40496-7

Contents

1. Introduction

The tachocline is a thin shell inside the Sun where the rotation pattern changes strongly. Beneath the tachocline the solar rotation is rather uniform. Above the tachocline, the rotation rate varies with latitude to decrease from the equator to the poles. Inside the tachocline, a sharp transition from differential to uniform rotation occurs with increasing depth. The tachocline was discovered by probing the internal structure of the Sun with observations of its global oscillations. The helioseismology provided in particular the angular velocity distribution inside the Sun shown in figure 1 (Kosovichev *et al* 1997; Schou *et al* 1998; Wilson *et al* 1997).

The strong rotational shear inside the tachocline is believed to be important for the solar magnetic activity (Hughes *et al* 2007). Even the solar cycle may originate from the tachocline or its vicinity (Rüdiger and Brandenburg 1995). Also other stars with convective envelopes will possess tachoclines. Strong differences in the magnetic activity between fully convective stars which cannot have tachoclines and solar-type stars with their convective envelopes can then be expected (cf Donati *et al* (2007)).

The solar tachocline parameters are well known from helioseismology. The tachocline thickness is about 4% of the solar radius, its midpoint radius is $(0.692 \pm 0.005)R_\odot$, and it is slightly prolate in shape (Antia *et al* 1998; Charbonneau *et al* 1999b; Kosovichev 1996). The tachocline is located mainly if not totally beneath the base of the convection zone at $R_{\rm in} = 0.713R_\odot$ (Basu and Antia 1997; Christensen-Dalsgaard *et al* 1991) in the uppermost radiative zone.

The given picture of the internal solar rotation suggests that some coupling must exist between the base of the convection zone and the inner radiative core. Otherwise, the magnetic-induced rotational braking of the Sun on *evolutionary* time-scales would produce a rapidly rotating core (Dicke 1970). Moreover, an even stronger link between low and high latitudes should operate immediately below the base of the convection zone in order to suppress the latitudinal rotation rate difference. The magnetic theory which explains the tachocline structure as a consequence of a weak internal magnetic field in the solar radiative interior provides both the links simultaneously (Rüdiger and Kitchatinov 1997). The present paper summarizes the basic

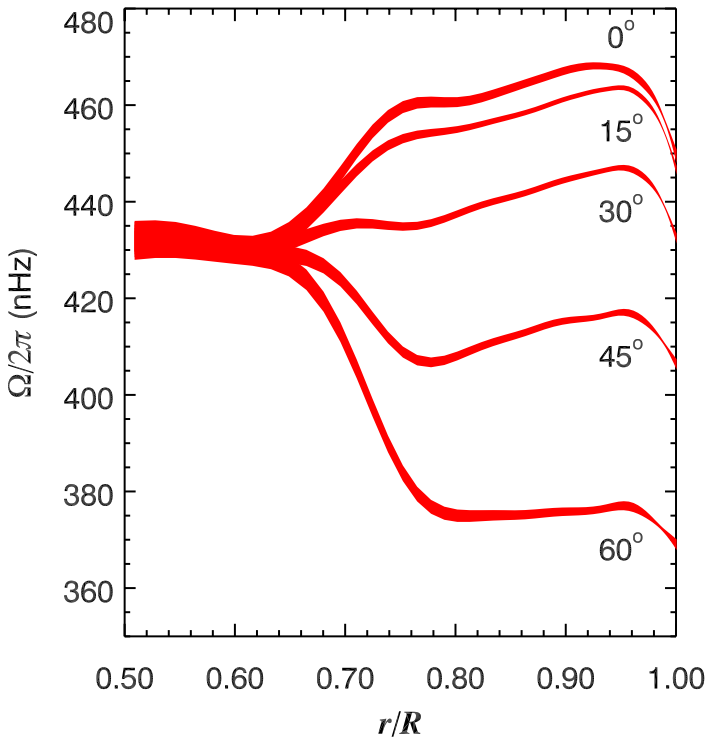

Figure 1. The internal solar rotation as a result of helioseismology. The radial profiles of the rotation rate $\Omega/2\pi$ are shown for several latitudes. The lines are marked by the latitude values. The tachocline is a thin layer around $r/R_\odot \simeq 0.7$ where transition from latitude-dependent rotation to uniform rotation occurs. Graph courtesy of NSF's National Solar Observatory.

ideas of the magnetic theory and describes new results of numerical magnetohydrodynamics (MHD) to model the tachocline and probing the internal field structure. Other approaches have been recently reviewed by Gilman (2005) and Garaud (2007).

The tachocline parameters expected from its formation by a magnetic field are estimated in the next section using a simplified model of tachocline in Cartesian geometry. Section 3 formulates the equations of the tachocline model and shows their solution for prescribed geometry of the fossil magnetic field within the radiative core. The role of a meridional flow penetrating the uppermost region of the radiative core from the convection zone is discussed in section 4. Also in this section, the eigenmodes of the internal poloidal field are computed under the influence of the penetrating flow. Tachocline models with consistently defined internal field modes are discussed in section 5. In the final section 6 a first step is presented towards understanding the stability of the solar tachocline. In a *hydrodynamical* approach the 2D theory of Watson (1981) for the stability of latitudinal differential rotation is reformulated in 3D with surprising results. The modes with rather small radial wavelengths are most unstable.

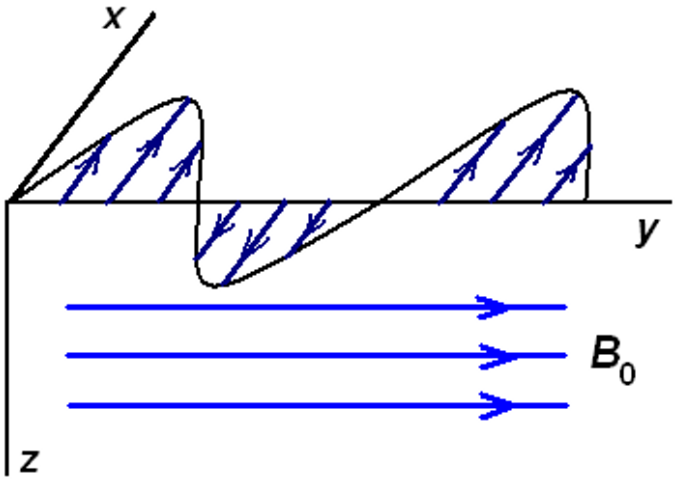

Figure 2. A shear flow is prescribed at $z = 0$. Its penetration into the region of $z > 0$ where the magnetic field $\mathbf{B}_0$ exists mimics the magnetic tachocline.

2. Heuristic approach

The basic parameters of the magnetic tachocline can be estimated with a simplified shear flow model in Cartesian geometry as sketched in figure 2. The Cartesian coordinates x, y and z may correspond to azimuth, latitude and depth beneath the base of the convection zone. The plane of $z = 0$ mimics the bottom of the convection zone where a shear flow $\boldsymbol{u} = (U(y, z), 0, 0)$ imitating the differential rotation is prescribed by

$$U = U_0 \sin(ky). \tag{1}$$

In a steady-state, penetration of the shear flow into the radiative zone of $z > 0$ where a uniform (poloidal) field $\boldsymbol{B}_0$ along the y-axis is present imitates the magnetic tachocline. The shear flow produces a toroidal x-component $B(y, z)$ of the field so that $\boldsymbol{B} = (B(y, z), B_0, 0)$.

The equations for the steady azimuthal components of both magnetic and velocity fields are then

$$\nu\left(\frac{\partial^2 U}{\partial y^2} + \frac{\partial^2 U}{\partial z^2}\right) + \frac{B_0}{\mu_0 \rho}\frac{\partial B}{\partial y} = 0, \quad \eta\left(\frac{\partial^2 B}{\partial y^2} + \frac{\partial^2 B}{\partial z^2}\right) + B_0\frac{\partial U}{\partial y} = 0, \tag{2}$$

where ν is the viscosity and η the magnetic diffusivity. The boundary condition for the flow is given by (1). For the toroidal field we impose the vacuum condition $B = 0$ at $z = 0$ motivated by the very large turbulent magnetic diffusivity inside the convection zone compared with the microscopic diffusivity of the radiative interior. The remaining two conditions require U and B to vanish for $z \to \infty$.

The solutions of equations (2) read

$$\begin{aligned} U(y, z) &= U_0 \exp(-\lambda_1 kz)\cos(\lambda_2 kz)\sin ky, \\ B(y, z) &= \sqrt{\mu_0 \rho} U_0 Pm^{1/2} \exp(-\lambda_1 kz)\sin(\lambda_2 kz)\cos ky, \end{aligned} \tag{3}$$

where $Pm = \nu/\eta$ is the magnetic Prandtl number. The parameters

$$\lambda_1 = \left(1 + \mathrm{Ha}^2\right)^{1/4} \cos\left(\tfrac{1}{2}\mathrm{arc\,tan}(\mathrm{Ha})\right) \tag{4}$$

and

$$\lambda_2 = \left(1 + \mathrm{Ha}^2\right)^{1/4} \sin\left(\tfrac{1}{2}\mathrm{arc\,tan}(\mathrm{Ha})\right) \tag{5}$$

depend on the Hartmann number

$$\mathrm{Ha} = \frac{B_0}{k\sqrt{\mu_0 \rho \nu \eta}}, \tag{6}$$

which is the basic parameter of the whole theory.

For $\mathrm{Ha} = 0$ the equations give $\lambda_1 = 1$, $\lambda_2 = 0$, and (3) converts into the nonmagnetic solution $U = U_0 \mathrm{e}^{-kz} \sin ky$. The shear flow penetrates deep inside the $z > 0$ region in this case. No slender tachocline can thus be formed without magnetic fields.

With solar parameters one finds $\mathrm{Ha} \simeq 10^7 B_0$ (B_0 in G) just below the convection zone. Very large Ha can thus be expected. For this case, $\lambda_1 = \lambda_2 = \sqrt{\mathrm{Ha}/2}$, and the solution (3) provides two important consequences.

1. The tachocline thickness, D_{tach}, is strongly reduced compared to its nonmagnetic value, D_0,

$$D_{\mathrm{tach}} = D_0 \sqrt{\frac{2}{\mathrm{Ha}}} \simeq \sqrt{\frac{D_0}{B_0}} \left(\mu_0 \rho \nu \eta\right)^{1/4}. \tag{7}$$

   The tachocline is so thin because its extension in the z-direction is only due to viscous stress while the smoothing in the y-direction is provided by the much stronger Maxwell stress.

2. The amplitude

$$B = U_0 \sqrt{\mu_0 \rho\, Pm} \tag{8}$$

   of the toroidal magnetic field in the steady tachocline does not depend on the poloidal field strength. The ratio of magnetic to kinetic energy in the tachocline equals Pm which is a small number for microscopic diffusion (see figure 3).

   In terms of the Alfvén velocity, $V_{\mathrm{A}} = B/\sqrt{\mu_0 \rho}$, one finds

$$V_{\mathrm{A}} = \sqrt{Pm}\, U_0. \tag{9}$$

Equation (8) means $B \lesssim 1000\,\mathrm{G}$ for the Sun. After (7) even a weak poloidal field of only $B_0 \sim 10^{-3}$ G can reduce D_{tach} below 5% of the solar radius. Equation (7) also holds when B_0 is of other origin than being a fossil field of the radiative core. If B_0 is the poloidal field of the solar cycle which diffuses into the core due to turbulent mixing (Forgács-Dajka and Petrovay 2002) ν and η must be replaced by their turbulent values. As the magnetic Prandtl number is no longer small, the resulting toroidal magnetic field after (9) becomes *much* stronger than 1000 G and their stability against nonaxisymmetric perturbations after Tayler (1973) and Vandakurov (1972) must be checked.

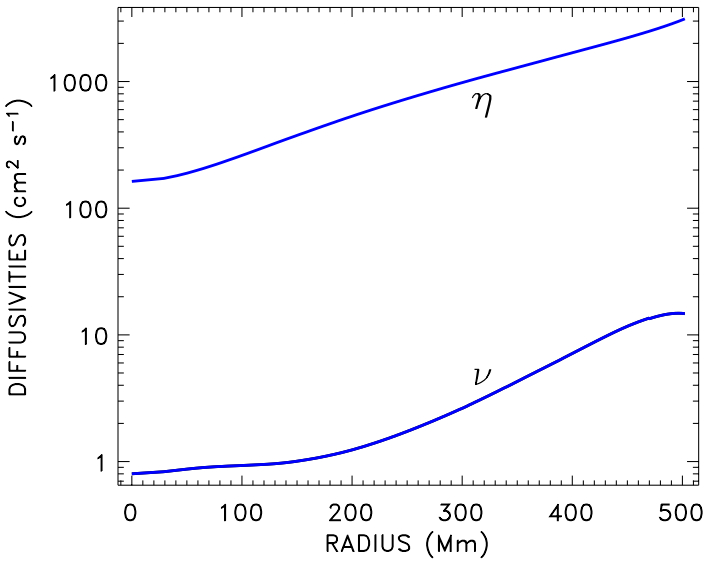

Figure 3. Radial profiles of magnetic diffusivity (15) and viscosity (17) calculated with the solar structure model by Stix and Skaley (1990).

3. Tachocline model in spherical geometry

The tachocline equations may be formulated for the axial symmetry. In this case the magnetic field can be expressed in terms of the toroidal field, B, and the potential A of the poloidal field,

$$\boldsymbol{B} = \mathbf{e}_\phi B + \nabla \times \left(\mathbf{e}_\phi \frac{A}{r \sin\theta} \right), \tag{10}$$

where r, θ and ϕ are the spherical coordinates and $\mathbf{e}_\phi$ is the azimuthal unit vector. In the next section we shall show that the meridional flow is only significant for the structure of the poloidal field. It can thus be neglected in the tachocline equations. Here the only flow is the rotation with the nonuniform angular velocity $\Omega(r, \theta)$.

The equation for the poloidal field decouples from the rest of the equation system. The poloidal field is discussed in the next section but here the field is assumed as given. The tachocline is described by the equations for the toroidal field B and the angular velocity Ω, i.e.

$$\frac{\eta}{r} \frac{\partial}{\partial \theta} \left(\frac{1}{\sin\theta} \frac{\partial (B \sin\theta)}{\partial \theta} \right) + \frac{\partial}{\partial r} \left(\eta \frac{\partial (Br)}{\partial r} \right) = \frac{\partial (A, \Omega)}{\partial (r, \theta)}, \tag{11}$$

and

$$\frac{\rho \nu}{\sin^3\theta} \frac{\partial}{\partial \theta} \left(\sin^3\theta \frac{\partial \Omega}{\partial \theta} \right) + \frac{1}{r^2} \frac{\partial}{\partial r} \left(r^4 \rho \nu \frac{\partial \Omega}{\partial r} \right) = \frac{1}{\mu_0 r^2 \sin^3\theta} \frac{\partial (A, Br \sin\theta)}{\partial (r, \theta)}. \tag{12}$$

The differential rotation of the convection zone imposes the angular velocity profile on the top boundary for which the expression

$$\Omega = 2.9 \left(1 - 0.15 \cos^2\theta \right) \ \mu \,\mathrm{rad\,s^{-1}}, \tag{13}$$

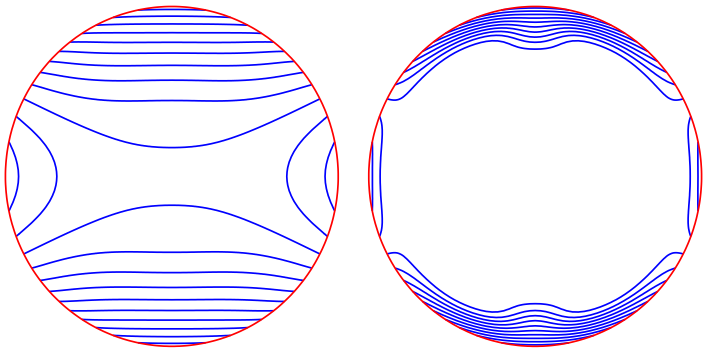

Figure 4. Isolines of the angular velocity inside the radiative core for the poloidal field model (18) with $q = 5$. The outer circle is the base of the convection zone. Left: $B_\mathrm{p} = 0$, no tachocline. Right: $B_\mathrm{p} = 0.01$ G, tachocline is formed.

at $r = R_\mathrm{in}$ by Charbonneau *et al* (1999a) is used. The remaining boundary conditions are the vacuum condition for the toroidal field on the top and the regularity conditions for the fields at $r = 0$, i.e.

$$B|_{r=R_\mathrm{in}} = B|_{r=0} = \left.\frac{\partial\Omega}{\partial\theta}\right|_{r=0} = 0. \tag{14}$$

The diffusivity profiles are shown in figure 3. We do not expect turbulence in the radiative core and shall use, therefore, the microscopic magnetic diffusivity

$$\eta = 10^{13} T^{-3/2}\,\mathrm{cm}^2\,\mathrm{s}^{-1}, \tag{15}$$

and the viscosity

$$\nu = \nu_\mathrm{micro} + \nu_\mathrm{rad} \tag{16}$$

with

$$\nu_\mathrm{micro} = 1.2 \times 10^{-16} \frac{T^{5/2}}{\rho}\mathrm{cm}^2\mathrm{s}^{-1}, \quad \nu_\mathrm{rad} = 2.5 \times 10^{-25} \frac{T^4}{\kappa\rho}\mathrm{cm}^2\mathrm{s}^{-1} \tag{17}$$

(Kippenhahn and Weigert 1994) including molecular (ν_micro) and radiative (ν_rad) parts; where κ is the opacity.

The equations (11) and (12) with the boundary conditions (13) and (14) provide the tachocline solutions if the poloidal field is known. For a first view the particular field model

$$A = B_\mathrm{p} \frac{r^2}{2} \left(1 - \frac{r}{R_\mathrm{in}}\right)^q \sin^2\theta \tag{18}$$

with $q > 1$ is used to probe whether slender tachoclines can be found. B_p is the free amplitude of the poloidal field. Figure 4 compares the patterns of radiative zone rotation computed with zero magnetic field and with $B_\mathrm{p} = 0.01$ G. B_p is the *maximum* strength of the poloidal field inside the core. The maximum is attained in the core centre. The field in the tachocline region is much weaker. Even this rather weak field suffices to produce a very strict and slender tachocline.

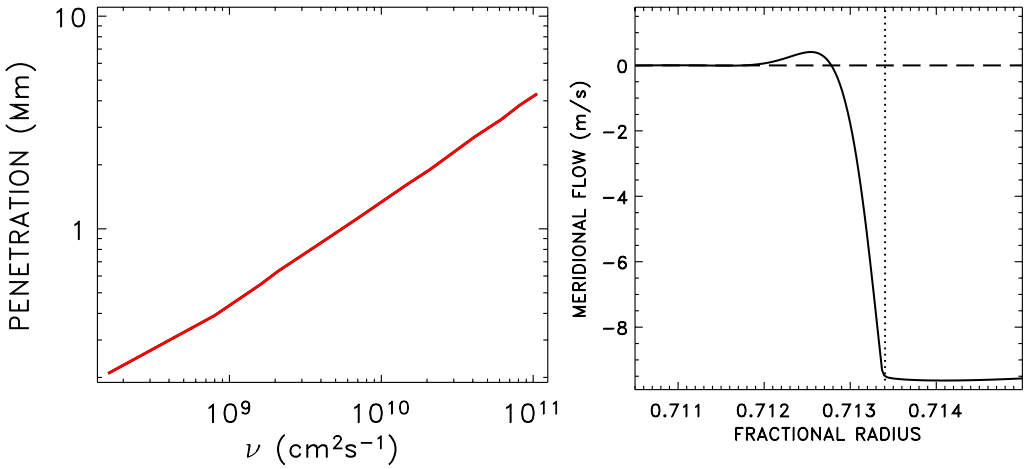

Figure 5. Left: depth of meridional flow penetration into the radiative core as a function of the viscosity below the convection zone. Right: meridional velocity in the penetration region at 45° latitude for $\nu = 1.3 \times 10^9\,\mathrm{cm^2\,s^{-1}}$. The vertical dotted line marks the bottom of the convection zone.

4. Magnetic field confinement by meridional flow

The tachocline model with a prescribed poloidal field is not yet consistent. We have shown that the model is not very sensitive to the poloidal field amplitude. Even a weak field can produce tachoclinic structures. The model is, however, very sensitive to the field geometry. A tachocline can only be produced if the field lines are almost horizontal near the top of the radiative zone (MacGregor and Charbonneau 1999). Steady rotation and steady magnetic fields can be realized in highly conducting fluids only with constant angular velocity along the field lines (Ferraro 1937). Therefore, the open field geometry with field lines crossing the boundary between convection and radiative zones cannot be appropriate for tachocline formation. The poloidal field prescribed by equation (18) is of the closed type. The field can, however, change to an open structure due to magnetic diffusion (Brun and Zahn 2006). We shall show that even a small *penetration* of meridional flow from the convection zone into the radiative core produces the confined field geometry required for the tachocline formation (Kitchatinov and Rüdiger 2006). If the electric conductivity in the core is high enough then the flow has massive consequences and the poloidal field lines in the penetration zone become parallel to the meridional flow (cf Mestel (1999)).

4.1. Penetration of meridional circulation

A global poleward flow observed on the solar surface (Komm *et al* 1993) persists to a depth of at least 12 Mm (Zhao and Kosovichev 2004). There must be a return flow towards the equator somewhere deeper. Theoretical models indeed predict an equatorward flow of $\sim$10 m s^{-1} at the base of the convection zone (Kitchatinov and Rüdiger 1999; Miesch *et al* 2000; Rempel 2005). This flow can penetrate beneath the bottom of the convection zone into the radiative core (figure 5). This penetration has been discussed recently in relation to dynamo models for solar activity (Gilman and Miesch 2004; Nandy and Choudhuri 2002; Rüdiger *et al* 2005).

The penetration results from the viscous drag imposed by the meridional flow at the base of the convection zone on the fluid beneath, and this is opposed by the Coriolis force. The Ekman balance leads to the estimation of the penetration depth

$$D_{\rm pen} \sim \sqrt{\frac{\nu}{\Omega}}, \tag{19}$$

(Gilman and Miesch 2004). The plot in the left of figure 5 is approximated well by $D_{\rm pen} \simeq 2.3\sqrt{\nu/\Omega}$ or, equivalently, by

$$D_{\rm pen} = 1400\sqrt{\nu}\,{\rm cm}, \tag{20}$$

for solar parameters and ν in cgs.[4] The penetration distance is about 100 m for the microscopic viscosity value and remains shorter than 1000 km for any reasonable value of eddy viscosity. The distance is always small even compared to the tachocline depth, i.e. $D_{\rm pen} \ll D_{\rm tach}$.

But this shallow penetration is of high relevance for the geometry of the internal poloidal field. The ratio of the diffusion time for the magnetic field across the penetration layer ($\tau_{\rm diff} = D_{\rm pen}^2/\eta$) to the characteristic time of induction of a latitudinal magnetic field from a radial one ($\tau_{\rm s} = D_{\rm pen}/u^{\rm m}$) gives the magnetic Reynolds number

$$Rm = \frac{D_{\rm pen}u^{\rm m}}{\eta} \simeq 10^6 \times \frac{Pm}{\sqrt{\nu}}, \tag{21}$$

where equation (20) for $D_{\rm pen}$ is applied, $u^{\rm m} \simeq 10\,{\rm m\,s^{-1}}$ for the meridional velocity is used and the viscosity is measured in ${\rm cm^2\,s^{-1}}$. For microscopic diffusivities with $Pm \simeq 5 \times 10^{-3}$ (figure 3), this Reynolds number is large, $Rm \sim 10^3$, and it remains above this value with eddy diffusivities ($Pm \sim 1$) up to $10^6\,{\rm cm^2\,s^{-1}}$. The large ratio (21) means that the latitudinal field inside the penetration layer is large compared to the radial field component so that the field has just the confined geometry required for the tachocline formation. With eddy diffusivities of $10^{12}\,{\rm cm^2\,s^{-1}}$ the Reynolds number (21) would sink to unity, so that only in this case the influence of penetration on the internal field geometry becomes weak.

The ratio of $\tau_{\rm diff}$ to the advection time $\tau_{\rm adv} = R_{\rm in}/u^{\rm m}$,

$$\frac{\tau_{\rm diff}}{\tau_{\rm adv}} = \frac{D_{\rm pen}}{R_{\rm in}} Rm \simeq 0.03\, Pm, \tag{22}$$

(with equation (21)) is always small independent of whether microscopic or eddy diffusion applies. If the tachocline is stable in the hydrodynamic regime (see section 6) the microscopic diffusivities should be used. The small ratio (22) justifies the neglect of the meridional flow in the tachocline equation (11). The diffusion time $\tau_{\rm diff}$ is so short that the penetration layer cannot be dynamo-relevant. Possibly, the configuration of the internal poloidal field is the only process for which the penetration of the meridional circulation into the stable radiative zone is important.

[4] $D_{\rm pen}$ of figure 5 was defined as distance from the convection zone bottom to the position where the meridional flow falls to zero.

4.2. A model of the poloidal field

For axisymmetric flows and fields the equation for poloidal magnetic field decouples from the tachocline equations (11) and (12) reads

$$\frac{\partial A}{\partial t} = -\frac{u_\theta}{r}\frac{\partial A}{\partial \theta} - u_r\frac{\partial A}{\partial r} + \eta\frac{\partial^2 A}{\partial r^2} + \frac{\eta}{r^2}\sin\theta\frac{\partial}{\partial\theta}\left(\frac{1}{\sin\theta}\frac{\partial A}{\partial\theta}\right), \tag{23}$$

where $\boldsymbol{u}$ is the velocity field. The vacuum boundary condition for the poloidal field can be applied on the top of the radiative zone because of the very large turbulent diffusivity in the convection zone,

$$\frac{\partial A}{\partial r} = \left(\frac{\partial A}{\partial r}\right)_{\rm vac} \quad \text{at } r = R_{\rm in}. \tag{24}$$

This condition is usually formulated in terms of a Legendre polynomial expansion

$$\begin{aligned} A(r,\theta) &= \sin\theta\sum_{n=1}^{\infty} A_n(r)\, P_n^1(\cos\theta), \\ \left(\frac{\partial A}{\partial r}\right)_{\rm vac} &= -\frac{\sin\theta}{r}\sum_{n=1}^{\infty} n A_n(r)\, P_n^1(\cos\theta). \end{aligned} \tag{25}$$

The second boundary condition is $A = 0$ at $r = 0$.

The velocity $\boldsymbol{u}$ can be written in terms of the streamfunction ψ as

$$\boldsymbol{u} = \left(\frac{1}{\rho r^2\sin\theta}\frac{\partial\psi}{\partial\theta}, -\frac{1}{\rho r\sin\theta}\frac{\partial\psi}{\partial r},\ r\sin\theta\,\Omega\right). \tag{26}$$

The meridional flow in the bulk of the radiative core is very slow. The characteristic time of the Eddington–Sweet circulation exceeds even the solar age (Tassoul 2000). Only the flow penetrating from the convection zone is thus significant for the tachocline. The streamfunction ψ of the penetrating flow drops to zero at a small depth of order $D_{\rm pen}$ inside the core. The function is, however, finite at the upper boundary of the core where it scales as

$$\psi(R_{\rm in},\theta) = u^{\rm m}\rho R_{\rm in} D_{\rm pen}\hat{\psi}(\theta), \tag{27}$$

where $\hat{\psi}$ is a dimensionless function of order unity. Here $u^{\rm m}$ is the meridional velocity amplitude at the boundary.

The penetration depth is so small even compared to the tachocline thickness that we are motivated to integrate equation (23) across the penetration layer instead of resolving this layer explicitly. Such an integration results in a reformulation of the top boundary condition which now reads

$$R_{\rm in}\frac{\partial A}{\partial r} - Rm\frac{\hat{\psi}(\theta)}{\sin\theta}\frac{\partial A}{\partial\theta} = R_{\rm in}\left(\frac{\partial A}{\partial r}\right)_{\rm vac}, \tag{28}$$

where Rm is the magnetic Reynolds number (21) and the rhs is defined in (25). For $Rm = 0$ the relation (28) reduces to the vacuum condition (24). The true Reynolds number is $Rm \sim 10^3$.

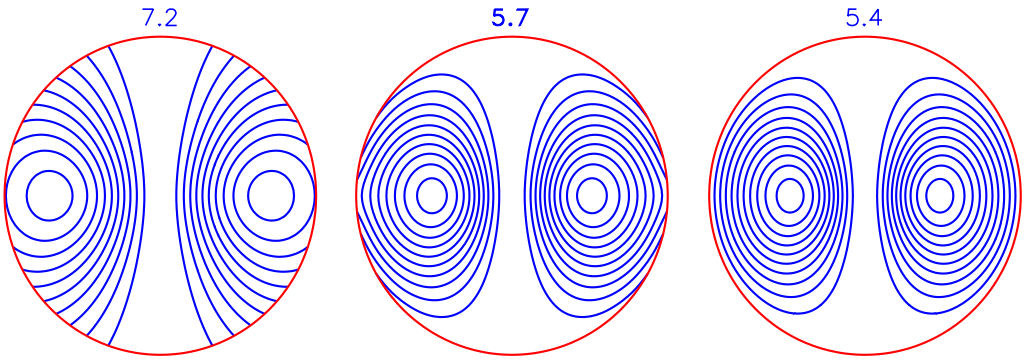

Figure 6. Field lines of the longest-living dipolar modes of the poloidal field for various Rm. The Reynolds number varies as $Rm = 0, 10, 1000$ from left to right. The outer circle is the base of convection zone. The decay times in Gyr are marked at the top.

The penetrating meridional flow is now included via the boundary condition (28) and the poloidal field can then be found by solving the eigenvalue problem

$$-\frac{A}{\tau} = \eta\frac{\partial^2 A}{\partial r^2} + \frac{\eta}{r^2}\sin\theta\frac{\partial}{\partial\theta}\left(\frac{1}{\sin\theta}\frac{\partial A}{\partial\theta}\right) \tag{29}$$

of the diffusion equation where the eigenvalue τ is the decay time of normal modes. The results discussed below were obtained in computations with the simplest streamfunction,

$$\hat{\psi}(\theta) = -\sin\theta P_2^1(\cos\theta), \tag{30}$$

where P_2^1 is the normalized Legendre polynomial (Kitchatinov and Rüdiger 2006).

The penetrating flow is expected to confine the internal poloidal field within the radiative core. The parameter

$$\delta\phi = \frac{\max|A(r,\theta)|_{r=R_{\rm in}}}{\max|A(r,\theta)|_{r\leqslant R_{\rm in}}} \tag{31}$$

can be used to estimate the field confinement. The $\delta\phi$ estimates the ratio of the magnetic flux through the surface of the core to the characteristic value of the flux within the core.

The linear equations (28) and (29) define the field structure but not its amplitude. The amplitude $B_{\rm p}$ of the poloidal field is thus a free parameter of the model.

4.3. Normal modes of the internal field

How the structure of the internal field changes towards a confined geometry for increasing Rm is shown in figure 6. The internal field computed with $Rm = 0$ has an open structure. Even a moderate flow with $Rm = 10$ already changes the field considerably towards a confined geometry. The internal field for the solar value $Rm = 10^3$, also shown in figure 6, is almost totally confined. Less than 1% of magnetic flux belongs to 'open' field lines in this case (figure 7).

Figure 6 displays the most slowly decaying dipolar modes. Other normal modes have smaller scales in radius or in latitude and also shorter decay times. The three modes following

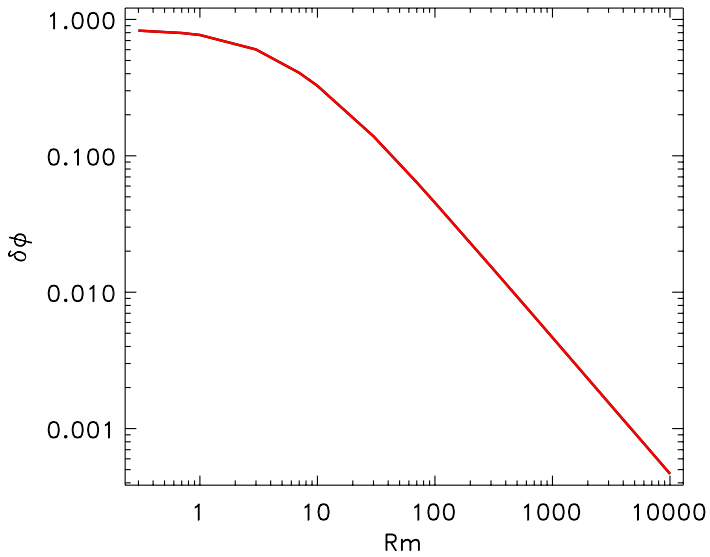

Figure 7. Confinement parameter (31) for the longest-living dipolar modes as a function of the magnetic Reynolds number Rm.

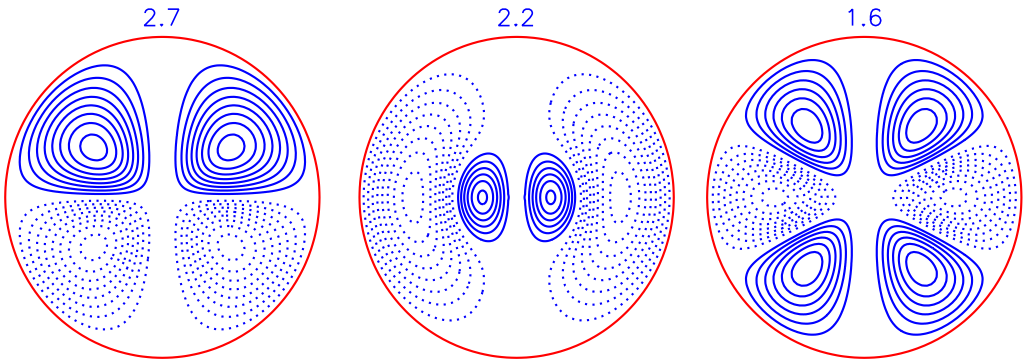

Figure 8. Normal modes of the internal field following the dipolar mode of figure 6 for shorter lifetimes. The decay times (in Gyr) are shown at the top. The confinement parameter (31) varies as 0.0051, 0.0073 and 0.0026 from left to right, $Rm = 1000$.

the longest-living dipole ordered for decreasing lifetimes are shown in figure 8. The higher-order modes also have a confined structure. The decay times of the given normal modes are long enough to allow tachocline computations with steady poloidal fields.

For sufficiently high Rm the direction of the penetrating meridional flow does not play a role. Also a flow from the equator to the poles makes efficient confinements of the internal field. The effect can be understood as a magnetic field expulsion from the region of circulating motion (Weiss 1966). The transition from convection zone to radiative core is treated as a sharp boundary in our model. A smooth decrease of the eddy diffusivity in the convection zone towards its base may also contribute to the field confinement via the diamagnetic effect of inhomogeneous turbulence (see Krause and Rädler (1980); Rüdiger and Hollerbach (2004)).

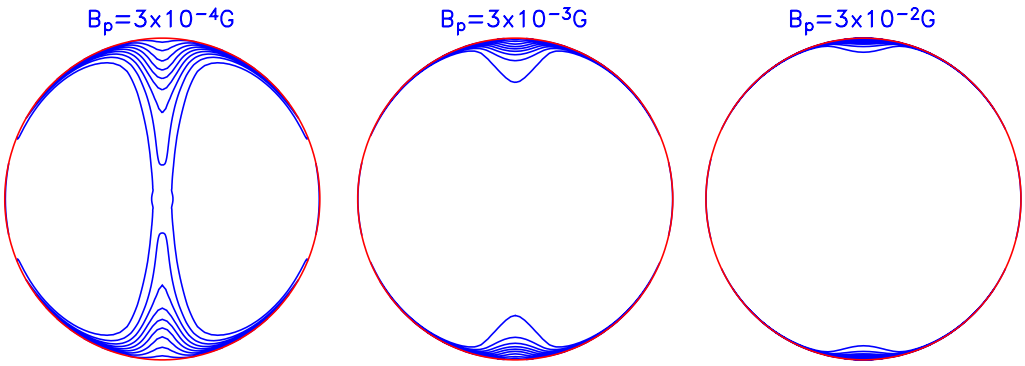

Figure 9. Angular velocity isolines in the radiative core computed with dipolar internal fields for $Rm = 1000$ for various poloidal field amplitudes (marked at the top).

5. Tachocline models

Figure 9 shows the angular velocity distributions inside the solar interior computed with dipolar eigenmodes of the internal field of various strengths. The dependence of the tachocline thickness on the poloidal field amplitude is shown in figure 10 where $D_{\rm tach}$ is defined as the depth of exponential decrease of the equator-to-pole difference in the angular velocity. Even such a weak field of 1 mG can produce a tachocline structure. The depth $D_{\rm tach}$ drops below 5% of the solar radius for $B_{\rm p} > 5$ mG.

The dependence of the tachocline thickness on the amplitude of the poloidal field is given in figure 10. It is very close to the estimate (7). The simulations also confirm the above finding that the toroidal field amplitude, $B_{\rm t} \simeq 100 \cdots 200$ G, hardly varies while the poloidal field amplitude changes by several orders of magnitude. Figure 10 suggests that the poloidal field amplitude should be about 8 mG to reproduce the observed small value of the tachocline thickness.

Also the higher-order modes given in figure 8 produce tachoclinic structures provided that the fields have the confined geometry which is always the case for $Rm \geqslant 100$.

Our results are rather robust. Figures 9 and 10 are valid for $Rm = 1000$. Already $Rm = 100$ suffices for the tachocline formation. For smaller Rm the poloidal field remains 'too open' for the formation of a tachocline. In other words, a meridional flow with minimum 1 m s^{-1} amplitude at the base of the convection zone is necessary for the magnetic tachocline theory to work. The very shallow penetration of the meridional flow from the convection zone into the radiative core influences the internal field geometry strongly enough and in such a way that the field becomes appropriate for the tachocline formation. We suggest that *a layer thinner than 1 Mm beneath the convection zone where a meridional flow of 1–10 m s^{-1} enters the solar radiative interior is responsible for the existence of the solar tachocline*.

6. Hydrodynamic stability: the Watson approach in 3D

Note that latitudinal differential rotation can be unstable even without magnetic field if the shear $\partial\Omega/\partial\theta$ is positive and sufficiently strong (Watson 1981). The critical value of 29% latitudinal shear found by Watson for the nonaxisymmetric mode with $m = 1$ resulted from a theory with

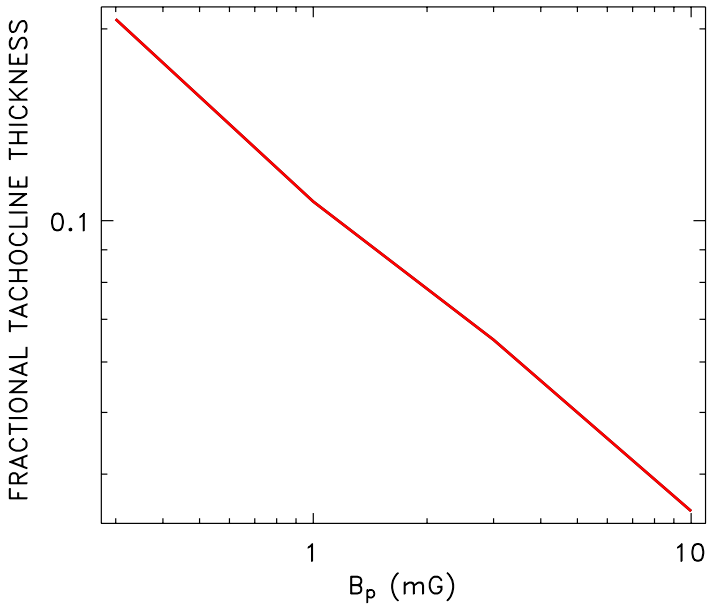

Figure 10. The fractional tachocline thickness as a function of the amplitude, B_p, of the internal poloidal field, $Rm = 1000$.

strong radial stratification but without any radial velocity. The value has also appeared in a 3D numerical consideration of marginal stability of a shell rotating fast enough with the rotation law

$$\Omega = \Omega_0 \left(1 - a \cos^2 \theta\right) \tag{32}$$

but of incompressible material (Arlt *et al* 2007). The critical shear increases to higher values, however, if the real rotation law (including its radial variations) of the solar tachocline is adopted. In this case the superrotation observed in the equatorial region of the Sun strongly stabilizes the shear instability.

In the present section the 2D approach by Watson is extended to 3D, i.e. to the inclusion of finite radial velocities and finite radial wavelengths. The stabilizing effect of a subadiabatic stratification is characterized by the buoyancy frequency N with

$$N^2 = \frac{g}{C_p} \frac{\partial S}{\partial r}, \tag{33}$$

where $S = C_v \log (P/\rho^\gamma)$ is the specific entropy of ideal gas. The Brunt–Väisälä frequency N in the solar radiative core is very large compared to Ω (see figure 11). The larger the N the more the radial fluctuations are suppressed by the 'negative' buoyancy force. Radial velocities should therefore be small. Our stability analysis is local in the radial dimension, i.e. we use Fourier modes $\exp(\mathrm{i}kr)$ in the short-wave approximation $kr \gg 1$. The analysis remains, however, global in horizontal dimensions.

Instabilities of rotating shear flows are slow compared to characteristic times of the compressive p-modes. Their growth rates are of order Ω or smaller. In the short-wave approximation the velocity field can be assumed as divergence-free ($\mathrm{div}\, \boldsymbol{u}' = 0$). The next

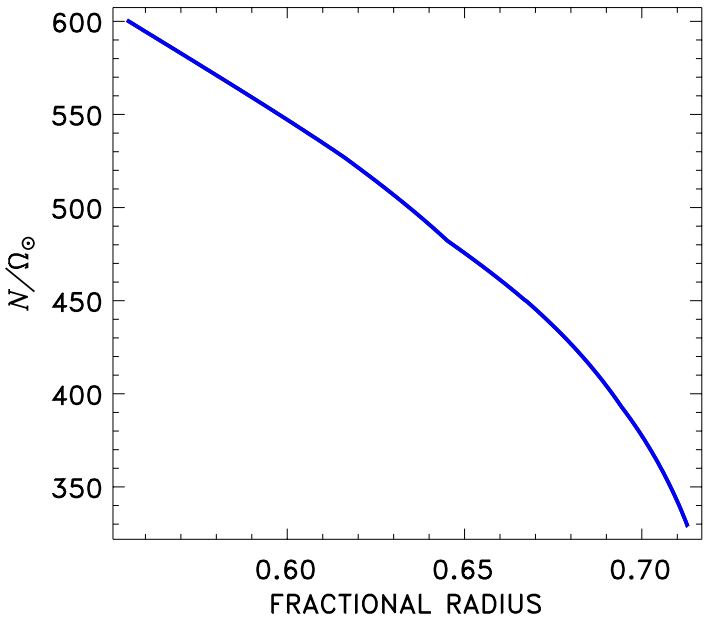

Figure 11. The buoyancy frequency (33) in the upper radiative core following the solar model of Stix and Skaley (1990).

assumption concerns the pressure. Local thermal disturbances occur at constant pressure so that $\rho'/\rho = -T'/T$ or $S' = -C_\mathrm{p}\rho'/\rho$ where perturbations have been marked by dashes. This assumption is again justified by the incompressible nature of the disturbances (Acheson 1978).

We start from the linearized equations for the velocity disturbances, i.e.

$$\frac{\partial \boldsymbol{u}'}{\partial t} + (\boldsymbol{u}\cdot\nabla)\,\boldsymbol{u}' + \left(\boldsymbol{u}'\cdot\nabla\right)\boldsymbol{u} = -\left(\frac{1}{\rho}\nabla p\right)' + \nu\Delta\boldsymbol{u}' \tag{34}$$

and entropy disturbances

$$\frac{\partial S'}{\partial t} + \boldsymbol{u}\cdot\nabla S' + \boldsymbol{u}'\cdot\nabla S = \frac{C_\mathrm{p}\chi}{T}\Delta T'. \tag{35}$$

The basic flow is the rotation law (32).

The perturbations of velocity are now expressed in terms of scalar potentials, i.e.

$$\boldsymbol{u}' = \frac{\boldsymbol{e}_r}{r^2}\mathcal{L}P - \frac{\boldsymbol{e}_\theta}{r}\left(\frac{1}{\sin\theta}\frac{\partial T}{\partial\phi} + \frac{\partial^2 P}{\partial r\partial\theta}\right) + \frac{\boldsymbol{e}_\phi}{r}\left(\frac{\partial T}{\partial\theta} - \frac{1}{\sin\theta}\frac{\partial^2 P}{\partial r\partial\phi}\right) \tag{36}$$

with the operator

$$\mathcal{L} = \frac{1}{\sin\theta}\frac{\partial}{\partial\theta}\sin\theta\frac{\partial}{\partial\theta} + \frac{1}{\sin^2\theta}\frac{\partial^2}{\partial\phi^2}. \tag{37}$$

The identities

$$r\left(\boldsymbol{r}\cdot\nabla\times\boldsymbol{u}'\right) = \mathcal{L}T, \qquad r^3\left(\boldsymbol{r}\cdot\nabla\times\nabla\times\boldsymbol{u}'\right) = -\left(\mathcal{L} + r^2\frac{\partial^2}{\partial r^2}\right)\mathcal{L}P \tag{38}$$

are used to reformulate the equations in terms of the potentials. It is a standard procedure. The radial component of the curled equation (34) gives the equation for the potential T of the toroidal flow. The radial component of the same equation curled twice gives the equation for the poloidal flow.

The perturbations are considered as Fourier modes in the form of $\exp(\mathrm{i}(-\omega t+m\phi+kr))$. For an instability the eigenvalue ω must possess a positive imaginary part. Only the highest order terms in kr for the same variable have been retained. The pressure term in the poloidal flow equation can be transformed as

$$\begin{aligned}\boldsymbol{r}\cdot\nabla\times\nabla\times\left(\frac{1}{\rho}\nabla p\right)' &= -\boldsymbol{r}\cdot\nabla\times\left(\frac{1}{\rho^2}(\nabla\rho)\times(\nabla p)\right)' \\ &= \frac{\boldsymbol{r}}{C_\mathrm{p}}\cdot\nabla\times\left(\frac{1}{\rho}(\nabla S)\times(\nabla p)\right)' = -\frac{\boldsymbol{r}}{C_\mathrm{p}}\cdot\nabla\times\left(\boldsymbol{g}\times\nabla S'\right) = \frac{g}{rC_\mathrm{p}}\mathcal{L}S'. \end{aligned} \tag{39}$$

In order to normalize the variables the time is measured in units of Ω_0^{-1} and the velocities are scaled with $r\Omega_0$. The remaining dimensionless variables are

$$V = \frac{k}{\Omega_0 r^2}P, \quad W = \frac{1}{\Omega_0 r^2}T, \quad s = \frac{\mathrm{i}krg}{C_\mathrm{p}rN^2}S', \quad \hat{\Omega} = \frac{\Omega}{\Omega_0}. \tag{40}$$

Now the equation for the poloidal flow reads

$$\begin{aligned}\hat{\omega}\,(\mathcal{L}V) = &-\hat{\lambda}^2\,(\mathcal{L}s) - \mathrm{i}\frac{\epsilon_\nu}{\hat{\lambda}^2}\,(\mathcal{L}V) - 2\mu\hat{\Omega}\,(\mathcal{L}W) - 2\left(1-\mu^2\right)\frac{\partial\left(\mu\hat{\Omega}\right)}{\partial\mu}\frac{\partial W}{\partial\mu} - 2m^2\frac{\partial\hat{\Omega}}{\partial\mu}W \\ &+ m\hat{\Omega}\,(\mathcal{L}V) + 2m\frac{\partial\left(\mu\hat{\Omega}\right)}{\partial\mu}V + 2m\left(1-\mu^2\right)\frac{\partial\hat{\Omega}}{\partial\mu}\frac{\partial V}{\partial\mu}\end{aligned} \tag{41}$$

with $\mu = \cos\theta$ and the normalized radial wavelength

$$\hat{\lambda} = \frac{N}{\Omega_0 kr}. \tag{42}$$

The first term on the rhs of (41) describes the stabilizing effect of the subadiabatic stratification. It vanishes for small $\hat{\lambda}$. Apart from this 'negative' buoyancy term, the wavelength only appears in the diffusive terms. The second term of the rhs includes the action of viscosity. Here and in the following we have used the quantities

$$\epsilon_\nu = \frac{\nu N^2}{\Omega_0^3 r^2}, \quad \epsilon_\chi = \frac{\chi N^2}{\Omega_0^3 r^2}, \tag{43}$$

for the dissipation parameters ν and χ. Their numerical values for the solar tachocline are

$$\epsilon_\nu \simeq 2\cdot 10^{-10}, \quad \epsilon_\chi \simeq 10^{-4}. \tag{44}$$

The third and the following terms in the right of (41) describe the influences of the basic rotation. Note that only latitudinal derivatives of Ω appear.

The complete system of equations also includes the equation for the toroidal flow,

$$\hat{\omega}\,(\mathcal{L}W) = -\mathrm{i}\frac{\epsilon_\nu}{\hat{\lambda}^2}\,(\mathcal{L}W) + m\hat{\Omega}\,(\mathcal{L}W) + (\mathcal{L}V)\,\frac{\partial}{\partial\mu}\left(\left(1-\mu^2\right)\hat{\Omega}\right) - mW\frac{\partial^2}{\partial\mu^2}\left(\left(1-\mu^2\right)\hat{\Omega}\right) + \left(\frac{\partial}{\partial\mu}\left(\left(1-\mu^2\right)^2\frac{\partial\hat{\Omega}}{\partial\mu}\right) - 2\left(1-\mu^2\right)\hat{\Omega}\right)\frac{\partial V}{\partial\mu}, \tag{45}$$

and the entropy equation

$$\hat{\omega}s = -\mathrm{i}\frac{\epsilon_\chi}{\hat{\lambda}^2}s + m\hat{\Omega}s + \mathcal{L}V. \tag{46}$$

For the Reynolds number

$$Re = \frac{\Omega r^2}{\nu}, \tag{47}$$

follows

$$Re = \frac{N^2/\Omega^2}{\epsilon_\nu}, \tag{48}$$

which with (44) is very large.

For positive latitudinal shear a in (32) the modes A1 and S2 become unstable for sufficiently large critical values a_{crit} (we use the notations Sm and Am for the eigenmodes with symmetric and antisymmetric profiles of W relative to the equator, m is the azimuthal wave number). Figure 12 shows the dependence of the a_{crit} on the normalized wavelength $\hat{\lambda}$. For large enough radial wavelengths the 29%-value of the Watson theory is reproduced. It is reduced, however, to $a = 0.21$ (21%) in our 3D calculations. We see that in contrast to the Watson approach the short radial scales rather than the long radial scales are preferred by the instability. The minimum a_{crit} appears for $\hat{\lambda} \simeq 0.6$, so that the characteristic wavelength of $\lambda \simeq 6$ Mm results as the most unstable mode of the solar tachocline. For shorter scales the instability for $m = 1$ disappears but modes with higher m remain still unstable for basically higher latitudinal shear a.

7. Concluding remarks

The presence of a meridional flow with an amplitude of a few metres per second at the bottom of the convection zone is shown as necessary for the magnetic tachocline model. The flow provides the confined geometry of the internal magnetic field (with field lines parallel to the outer spherical boundary) which is necessary for the tachocline formation. The bottom flow is also a key ingredient of advection-dominated dynamo models for the solar cycle (see Rüdiger and Hollerbach (2004) for detailed references). The flow is indeed predicted theoretically but its existence is not yet confirmed by observations. We hope, of course, that helioseismology will soon probe the deep meridional flow.

The polar cusps in the tachoclines of figure 9 are consequences of the assumed axisymmetry. This assumption may not be realistic. The penetrating meridional flow is, however, expected to confine even nonaxisymmetric fields to the core so that the fields should also be able to produce tachoclinic structures.

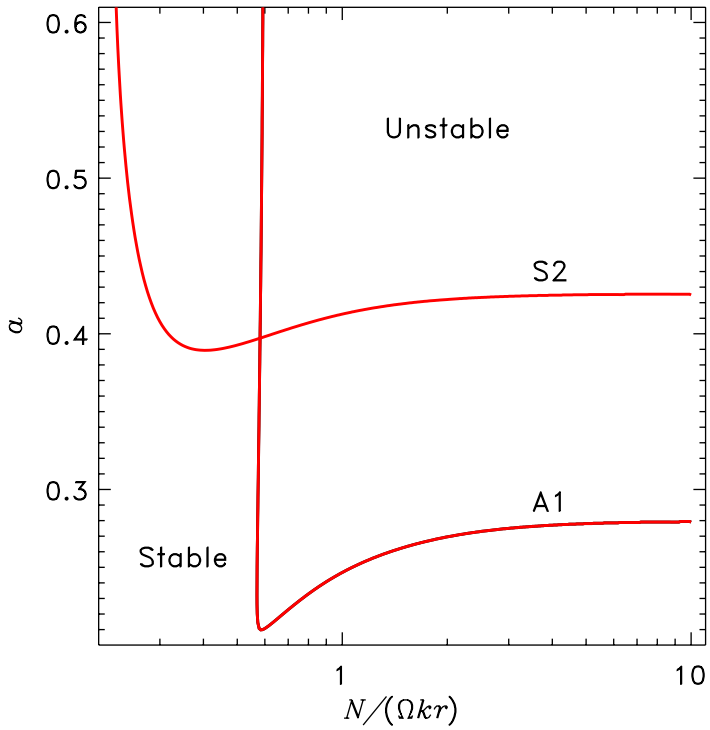

Figure 12. Stability map for the latitudinal differential rotation law (32). Most unstable are the perturbation modes with the vertical scale $\hat{\lambda} \simeq 0.6$. The critical magnitude of latitudinal shear is reduced to 0.21 compared to the 0.29 value of the large-wavelength limit.

The tachocline computations result in toroidal fields of 100–200 G, much stronger than the original poloidal fields. These toroidal fields can be subject to current-driven pinch-type instabilities. Hence, the question is whether the steady axisymmetric solutions of our model are stable against all the nonaxisymmetric disturbances. The threshold field strength for the instability were estimated to be of order $10^{2\cdots3}$ G (Arlt *et al* 2007; Kitchatinov and Rüdiger 2007; Spruit 1999) what is somewhat larger than the field amplitudes in our model.

It is important for the tachocline model that the magnetic Reynolds number (21) is large. This is true for microscopic diffusivities or for not too large eddy diffusivities up to about 10^8 cm^2 s^{-1}. The tachocline should, therefore, be stable or only mildly turbulent to allow poloidal field confinement by meridional flow. Some low level of turbulence may, however, even be necessary. The magnetic field is so efficient in producing tachocline structures that poloidal fields of only 1 G already lead to the tachocline thickness smaller than 1% of the solar radius. It is, however, observed that $D_{\rm tach} \simeq 0.04 R_\odot$. Hence, the internal poloidal field may indeed be small (Kitchatinov *et al* 2001) or, if it is not, some kind of instability prevents the tachocline thickness to reduce below the helioseismologically detected level.

The stability issue is a clear perspective for future tachocline studies. As a corresponding application we have extended in the preceding section the 2D theory of Watson (1981) for the hydrodynamic instability of latitudinal differential rotation to a 3D theory which allows us to find the critical values of the radial wavelengths. Now the critical wavelength of the unstable

mode with $m = 1$ is only 6 Mm while the critical latitudinal shear (see (32)) is reduced from 29 to 21%. This (linear) theory works with a hydrodynamic Prandtl number of order 10^{-6} and a very high Reynolds number of order 10^{15}.

Acknowledgments

We cordially acknowledge support by Deutsche Forschungsgemeinschaft and by the Russian Foundation for Basic Research (project 05-02-04015).

References

Acheson D J 1978 *Phil. Trans. R. Soc. Lond.* A **289** 459
Antia H M, Basu S and Chitre S M 1998 *Mon. Not. R. Astron. Soc.* **298** 543
Arlt R, Sule A and Rüdiger G 2007 *Astron. Astrophys.* **461** 295
Basu S and Antia H M 1997 *Mon. Not. R. Astron. Soc.* **287** 189
Brun A S and Zahn J-P 2006 *Astron. Astrophys.* **457** 665
Charbonneau P, Dikpati M and Gilman P A 1999a *Astrophys. J.* **526** 523
Charbonneau P, Christensen-Dalsgaard J, Henning R, Larsen R M, Schou J, Thompson M J and Tomczyk S 1999b *Astrophys. J.* **527** 445
Christensen-Dalsgaard J, Gough D O and Thompson M J 1991 *Astrophys. J.* **378** 413
Dicke R H 1970 *Ann. Rev. Astron. Astrophys.* **8** 297
Donati J-F *et al* 2007 *Preprint* astro-ph/0702159
Ferraro V C A 1937 *Mon. Not. Roy. Astron. Soc.* **97** 458
Forgács-Dajka E and Petrovay K 2002 *Astron. Astrophys.* **389** 629
Garaud P 2007 Dynamics of the Solar Tachocline *The Solar Tachocline* ed D W Hughes and N O Weiss (Cambridge: Cambridge University Press) p 147
Gilman P A 2005 *Astron. Nachr.* **326** 208
Gilman P A and Miesch M S 2004 *Astrophys. J.* **611** 568
Hughes D W, Rosner R and Weiss N O 2007 *The Solar Tachocline* (Cambridge: Cambridge University Press)
Kippenhahn R and Weigert A 1994 *Stellar Structure and Evolution* (Berlin: Springer)
Kitchatinov L L and Rüdiger G 1999 *Astron. Astrophys.* **344** 911
Kitchatinov L L, Jardine M and Cameron A C 2001 *Astron. Astrophys.* **374** 250
Kitchatinov L L and Rüdiger G 2006 *Astron. Astrophys.* **453** 329
Kitchatinov L L and Rüdiger G 2007 *Preprint* astro-ph/0701847
Komm R W, Howard R F and Harvey J W 1993 *Sol. Phys.* **147** 207
Kosovichev A G 1996 *Astrophys. J.* **469** L61
Kosovichev A G *et al* 1997 *Sol. Phys.* **170** 43
Krause F and Rädler K H 1980 *Mean-Field Magnetohydrodynamics and Dynamo Theory* (Oxford: Pergamon)
MacGregor K B and Charbonneau P 1999 *Astrophys. J.* **519** 911
Mestel L 1999 *Stellar Magnetism* (Oxford: Clarendon Press)
Miesch M S *et al* 2000 *Astrophys. J.* **532** 593
Nandy D and Choudhuri A R 2002 *Science* **296** 1671
Rempel M 2005 *Astrophys. J.* **622** 1320
Rüdiger G and Brandenburg A 1995 *Astron. Astrophys.* **296** 557
Rüdiger G and Kitchatinov L L 1997 *Astron. Nachr.* **318** 273
Rüdiger G and Hollerbach R L 2004 *The Magnetic Universe* (Berlin: Wiley-VCH)

Rüdiger G, Kitchatinov L L and Arlt R 2005 *Astron. Astrophys.* **444** L53
Schou J *et al* 1998 *Astrophys. J.* **505** 390
Spruit H C 1999 *Astron. Astrophys.* **349** 189
Stix M and Skaley D 1990 *Astron. Astrophys.* **232** 234
Tassoul J-L 2000 *Stellar Rotation* (Cambridge: Cambridge University Press)
Tayler R J 1973 *Mon. Not. R. Astron. Soc.* **161** 365
Vandakurov Yu V 1972 *Sov. Astron.* **16** 265
Watson M 1981 *Geophys. Astrophys. Fluid Dyn.* **16** 285
Weiss N O 1966 *Proc. R. Soc. Lond.* A **293** 310
Wilson P R, Burtonclay D and Li Y 1997 *Astrophys. J.* **489** 395
Zhao J and Kosovichev A G 2004 *Astrophys. J.* **603** 776